ACS APPLIED POLYMER MATERIALS

pubs.acs.org/acsapm Article

Perylene Diimide-Containing Dynamic Hyper-crosslinked Ionic Porous Organic Polymers: Modulation of Assembly and Gas Storage

Soujanya H. Goudar, Dhiraj S. Ingle, Rahul Sahu, Srinu Kotha, Sandeep K. Reddy, Deepu J. Babu, and Venkata Rao Kotagiri*

Cite This: *ACS Appl. Polym. Mater.* 2023, 5, 2097−2104 Read Online

ACCESS | Metrics & More | Article Recommendations | Supporting Information

ABSTRACT: A strategy to synthesize hyper-crosslinked polymers with strong visible-light absorption and abundant ionic sites is discussed. This is achieved in a one-pot reaction via the simultaneous Friedel−Crafts alkylation and quaternization reaction between α,α'-dibromo-*p*-xylene (DBX) and perylene diimide (PDI) substituted with *N*,*N*-dimethyl ethylene to result in hyper-crosslinked ionic polymers (HIPs). These HIPs display good surface areas with strong visible-light absorption (400−650 nm) and dispersibility in polar solvents like water and DMSO. Importantly, our experimental and theoretical studies indicate that **PDI-HIPs** possess a dynamic network with good uptake of water up to seven times their weight. Notably, PDI in **PDI-HIPs** is not only responsible for visible-light absorption but also acts as a probe to study their dynamic nature. Moreover, the presence of ultramicropores and CO_2-philic functional groups in **PDI-HIPs** renders good CO_2 uptake up to 2.11 mmol/g at 273 K despite their relatively low surface area.

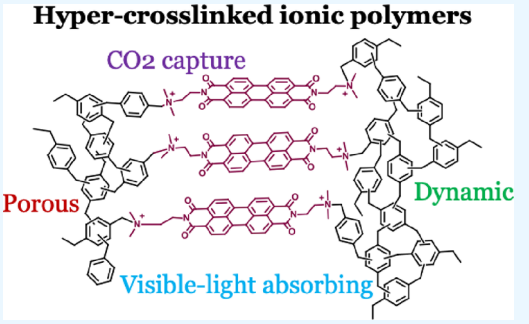

KEYWORDS: *hyper-crosslinked polymers, dynamic behavior, porous materials, perylene diimides, gas storage*

INTRODUCTION

Porous materials derived from organic linkers, known as porous organic polymers (POPs),[1,2] are promising candidates for gas storage[3−5] and separation,[6] catalysis,[7] sensing,[8] and energy storage.[9] POPs are further classified into various types such as covalent organic frameworks (COFs),[10] conjugated microporous polymers (CMPs),[11−13] porous aromatic frameworks (PAFs),[14] polymers of intrinsic microporosity (PIMs),[15] and hyper-crosslinked polymers (HCPs).[16−20] Among these, COFs are crystalline solids, and all others are mostly amorphous in nature. CMPs are an important class of POPs owing to their strong visible-light absorption in addition to their porosity. As a result, CMPs are widely explored for light-harvesting and photocatalytic applications.[21−24] Moreover, some of the CMP networks are dynamic in nature, which renders them superabsorbent properties.[24,25] Although some CMPs are synthesized without the aid of expensive metal catalysts,[26,27] most of the CMP syntheses requires the use of expensive metal catalysts to carry out polymerization reactions.[28] On the other hand, HCPs are synthesized using inexpensive starting materials and catalysts with tunable surface areas. For example, Tan et al. synthesized HCPs with a surface area up to 3000 m^2/g using inexpensive starting materials like benzene, triphenyl benzene, and dichloromethane in the presence of $AlCl_3$.[29] Li et al. reported the synthesis of multifunctional HCPs using inexpensive Scholl reaction conditions.[30] Adams et al. synthesized HCPs by crosslinking inexpensive starting materials such as toluene and anisole with formaldehyde dimethyl acetal using $FeCl_3$. The resultant HCPs display a good surface area, swelling in organic solvents, and uptake of chemical warfare agents.[31] Another advantage of HCPs is the incorporation of ionic functional groups into porous structures in one pot. For example, Wang et al. synthesized imidazolium-containing ionic HCPs using a combination of quaternization and Friedel−Crafts alkylation. The resultant polymers are explored for CO_2 capture and conversion.[32] Despite several interesting features, HCPs with strong visible-light absorption like CMPs and COFs are very rare.[33]

Introducing strong visible-light absorbing molecules in HCPs in addition to ionic sites would significantly broaden their applications. However, strategies to incorporate large π systems with strong visible-light absorption into HCPs are not well-explored. Although HCPs are synthesized by crosslinking perylene, their spectral coverage in the visible region is poor (<500 nm).[34] In this context, perylene diimide (PDI)-based π systems are very interesting owing to their interesting optoelectronic[35−37] and spintronic properties[38] with high chemical and thermal stability. Moreover, PDIs are also one

Received: December 6, 2022
Accepted: February 9, 2023
Published: February 22, 2023

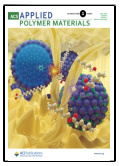

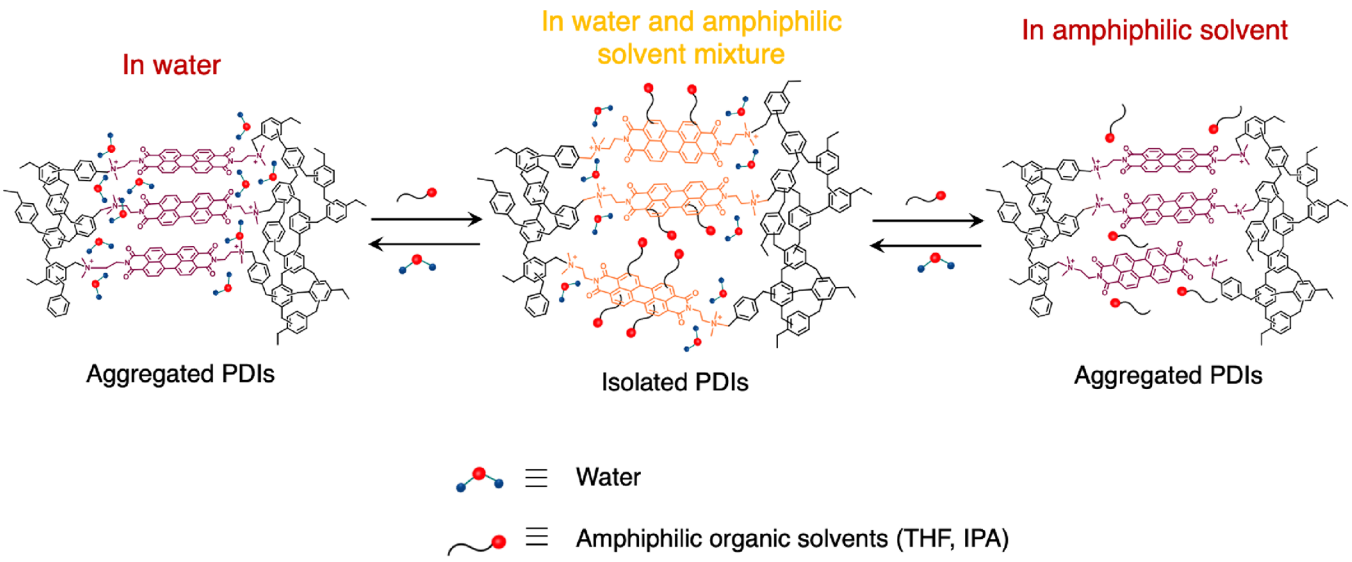

Figure 1. Schematic representation of modulation of stacking of perylene diimide (PDI) in **PDI-HIPs**.

of the promising candidates for creating functional soft materials via supramolecular self-assembly.[39,40] Furthermore, PDIs are also widely explored as an alternative to fullerenes in solar cells owing to their good electron transporting behavior and spectral coverage in the visible region (400−650 nm).[41−43] Owing to these interesting features, PDIs are also utilized as a building block in the synthesis of various POPs such as porous polyimides,[44−47] CMPs,[48] and COFs.[49] Hence, introducing PDIs into HCPs not only broadens their synthetic versatility but also introduces interesting functions. Moreover, due to the presence of flexible methylene bridges in HCPs, their network is expected to be dynamic in nature. However, no experimental studies were reported in this direction. Moreover, combining computational studies with the experiments would be helpful for a better understanding of the structure, stability, and dynamic behavior of polymers. In particular, computational tools such as molecular dynamics have proven useful in demonstrating the dynamic nature of PDI-based assemblies and the role of solvents.[50−55]

Here, we report a strategy to incorporate perylene diimides (PDIs) into the network of HCPs in a one-pot reaction to result in hyper-crosslinked ionic polymers (HIPs) containing PDIs. This is achieved by reacting α,α'-dibromo-*p*-xylene (DBX) and PDI substituted with *N*,*N*-dimethyl ethylene in different ratios in the presence of $FeCl_3$ in dichloroethane at 80 °C. During the reaction, in addition to Friedel−Crafts alkylation among benzene rings of DBX, quaternization also takes place on PDI side chains to result in PDI-incorporated HIPs having ammonium bromide groups. The resultant **PDI-HIPs** show a BET surface area of nearly 400 m^2/g with strong visible-light absorption. Due to the presence of ionic functional groups, **PDI-HIPs** show good dispersibility in polar solvents such as water, DMSO, and isopropanol with interesting solvent composition-controlled assembly−disassembly behavior (Figure 1). Moreover, due to the presence of ionic functional groups, **PDI-HIPs** swell in water with an uptake of up to 7 times their weight. These observations further indicate that **PDI-HIPs** possess a dynamic porous network. Owing to the porous structure endowed with polar functional groups, **PDI-HIPs** also show CO_2 uptake of more than 2 mmol/g at 273 K despite their relatively low surface area compared to other POPs explored for CO_2 capture.

RESULTS AND DISCUSSION

The synthesis of **PDI-HIPs** is shown in Scheme 1. A single-step reaction has been carried out where quaternization and

Scheme 1. Synthesis of PDI-HIPs in One Step Involving the Simultaneous Friedel−Crafts Alkylation and Quaternization Reactions

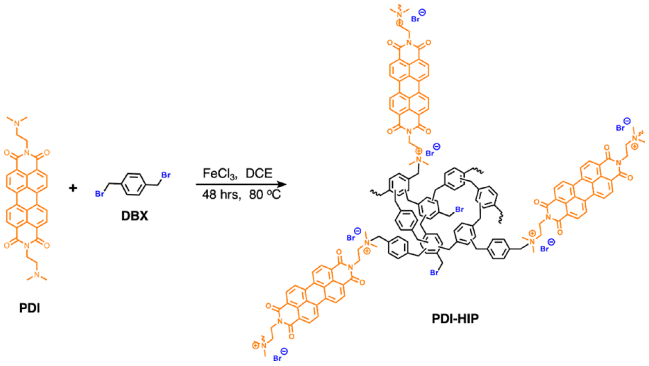

Friedel−Crafts alkylation occur simultaneously to get the desired **PDI-HIPs**. PDI having an *N*,*N*-dimethyl ethylene side chain and α,α'-dibromo-*p*-xylene (DBX) in different ratios are dissolved in 20 mL of DCE, and this mixture was degassed for 15 min by using N_2 gas followed by the addition of anhydrous $FeCl_3$ at room temperature under inert conditions (Table 1). The mixture was stirred at 80 °C for 48 h under a nitrogen (N_2) atmosphere to result in three polymers, **PDI-HIP-1**,

Table 1. Surface Area Analysis of PDI-HIPs

samples	no. of equivalents of PDI	no. of equivalents of DBX	BET surface area (m^2/g)	total pore volume (cc/g)
PDI-HIP-1	0.1	1.00	397	0.31
PDI-HIP-2	0.25	1.00	233	0.36
PDI-HIP-3	0.35	1.00	106	0.19

https://doi.org/10.1021/acsapm.2c02102
ACS Appl. Polym. Mater. 2023, 5, 2097−2104

PDI-HIP-2, and **PDI-HIP-3**. We noticed that the formation of the quaternary salt is negligible at room temperature. However, at 80 °C, the formation of the quaternary salt also significantly takes place under these reaction conditions. When we have performed a quaternization reaction alone (without anhydrous $FeCl_3$) in DCE at 80 °C using benzyl bromide and perylene diimide, we have obtained 73.8% isolated yield of benzyl ammonium-containing PDI (**B-PDI**) (see Supporting Information Section 3). Although it is difficult to estimate the exact reaction rates of Friedel−Crafts alkylation and quaternization, our observations indicate that under the reaction conditions used for the synthesis of **PDI-HIPs**, both the reactions take place simultaneously. All these **PDI-HIPs** are purified through Soxhlet extraction with methanol and chloroform. FT-IR spectra (Figure S3 and Table S2) of all **PDI-HIPs** show the C═O stretching frequency corresponding to imide groups around 1692 cm^{-1}. This confirms the successful insertion of PDI into the polymeric network. The peak at around 2927 cm^{-1} is attributed to the methylene linkage. The peak around 1346 cm^{-1} is due to the C−N stretching frequency. In the solid-state ^{13}C CP/MAS NMR spectra, all the three samples showed peaks in the range of 150 to 110 ppm corresponding to substituted and nonsubstituted aromatic carbon atoms (Figure 2a). The peak near 164 ppm is

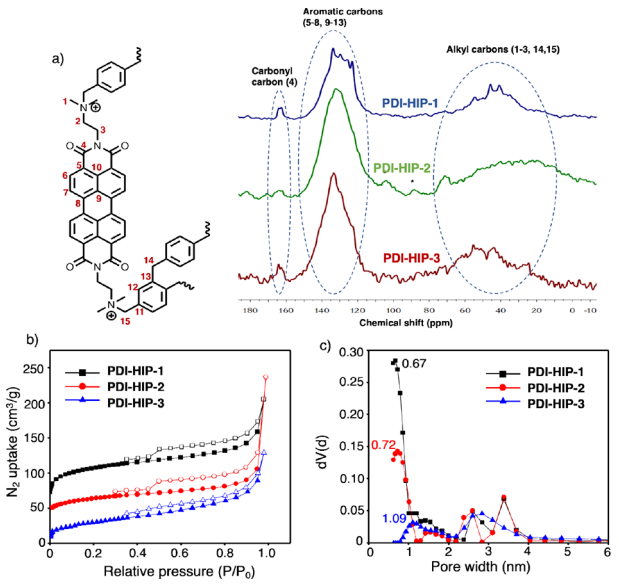

Figure 2. (a) Solid-state ^{13}C NMR spectra of **PDI-HIP-1**, **PDI-HIP-2**, and **PDI-HIP-3**. (b) N_2 sorption isotherms and (c) pore size distribution curves of **PDI-HIP-1**, **PDI-HIP-2**, and **PDI-HIP-3** measured at 77 K.

due to the carbonyl carbons of PDI. In the same way, the peaks from 70 to 20 ppm are due to the ethylene and methylene linkages in the polymer network. These observations further confirm the structure of **PDI-HIPs**. Since the carbon atoms of PDI and benzyl groups appear at different ppm, the appearance of ^{13}C CP/MAS NMR spectra for the three **PDI-HIPs** is different due to the change in the ratio of PDI and benzyl groups. We have also characterized **PDI-HIPs** using X-ray photoelectron spectroscopy (XPS). As expected, all **PDI-HIPs** show the characteristic peaks corresponding to C 1s, O 1s, N 1s, and Br 3d (Figure S4). However, in **PDI-HIP-3**, the characteristic peak corresponding to Fe is also observed. This indicates that, in **PDI-HIP-1** and **PDI-HIP-2**, Fe is effectively removed during purification via Soxhlet extraction. In **PDI-HIP-3**, probably due to the presence of a high PDI content, the high ionic sites might trap Fe (Figure S4). The thermal stability of all the **PDI-HIPs** was studied using thermogravimetric analysis (TGA). All the **PDI-HIPs** are stable up to 250 °C, and nearly 60% of the weight loss was observed by around 700 °C (Figure S5). The small weight loss (∼10%) below 250 °C could be due to the loss of volatile impurities and trapped water molecules.

The porous nature of the polymers was confirmed with the help of N_2 sorption isotherms at 77 K (Figure 2b). All three synthesized polymers exhibit type I−IV composite adsorption isotherms and the hysteresis loop of type H4.[56] The considerable increase in the uptake of N_2 at low relative pressure suggests the presence of micropores. The hysteresis observed further suggests the presence of mesopores in the structure confirming the porous nature of the polymers. Moreover, the steep uptake in the adsorption branch of the hysteresis loop is observed at partial pressures close to unity (Figure 2b).[56] This indicates that the observed mesopores are larger and could be due to the presence of agglomerates where condensation is happening in the interparticle voids. The presence of agglomerates with interparticle voids is further supported by the field-emission scanning electron microscopy (FE-SEM) images of **PDI-HIPs** (Figure S6). The porosity of the polymers is further determined through the pore size distribution (PSD) calculated by QSDFT considering the slit pore model (Figure 2c). For **PDI-HIP-1**, the pores are centered at 0.67, 2.60, and 3.38 nm with a total pore volume of 0.31 cc/g. The calculated BET surface area of **PDI-HIP-1** is the highest among all three polymers, which is 397 m^2/g. For **PDI-HIP-2**, the PSD shows the pores at 0.72, 2.60, and 3.38 nm with a total pore volume of 0.36 cc/g and a surface area of 233 m^2/g. The **PDI-HIP-3**, which was synthesized by using 0.35 equiv of PDI, has pores centered at 1.09, 2.60, and 2.84 nm with a total pore volume of 0.19 cc/g and a surface area of 106 m^2/g. The BET surface area of the polymers shows a decreasing trend (see Table 1) when the PDI equivalents increase, which could be due to the reduction in crosslinking among DBX molecules resulting in decreasing the surface area. Since PDI is a bigger molecule than DBX, when PDI equivalents are increased, more space will be created between the DBX molecules. As a result, the extent of crosslinking between the DBX molecules decreases. So, the amount of PDI plays a major role in surface area variation.

Due to the presence of ionic functional groups in **PDI-HIPs**, they form good dispersions in polar solvents like DMSO and water.[57] Recently, we reported that ionic π systems show supramolecular depolymerization behavior in the mixture of two poor solvents.[50] For example, for PDI-based ionic π systems, water and amphiphilic organic solvents (THF and IPA) are poor solvents as PDIs exist in the assembled form in these solvents. However, in the mixtures of water and amphiphilic solvents, PDIs disassemble and exist as monomers.[50] If **PDI-HIP** networks are dynamic, they also should show similar assembly−disassembly behavior depending on the solvent composition. However, so far, there are no reports that study the dynamic nature of HIPs and HCPs. Hence, we have explored the dynamic behavior of **PDI-HIPs** (0.025 mg/mL) in water, IPA, THF, and their mixtures by probing the absorption and emission changes of PDIs. The absorption spectra of **PDI-HIPs** in water show the peaks corresponding to the PDI core in the range of 400 to 600 nm (Figure 3a and

https://doi.org/10.1021/acsapm.2c02102
ACS Appl. Polym. Mater. 2023, 5, 2097−2104

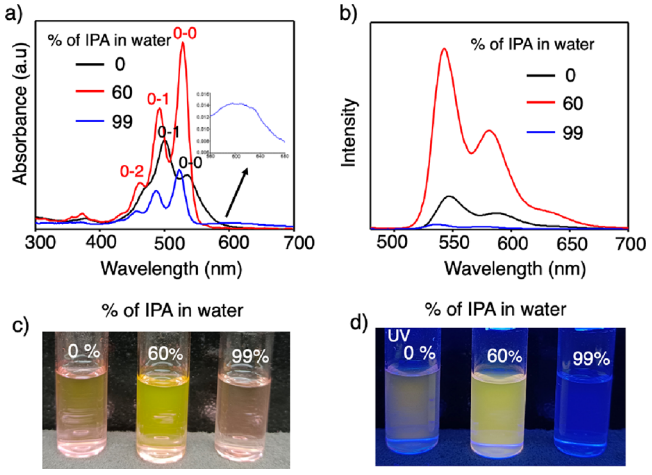

Figure 3. (a) Electronic absorption spectra and (b) emission spectra (λ_{ex} = 470 nm) of **PDI-HIP-1** (0.025 mg/mL) in water having different vol % of IPA. Photographs of **PDI-HIP-1** (0.025 mg/mL) in water having different vol % of IPA (c) under normal and (d) UV light.

Figures S7−S10). The appearance of absorption spectra indicates the presence of face-to-face stacking of PDIs in the **PDI-HIPs** as the ratio of absorbance of the 0−0 transition to the 0−1 transition is 0.5 (<1). Interestingly, when the vol % of IPA gradually increases in water, PDIs in the **PDI-HIPs** undergo disassembly, and at 60 vol % of IPA in water, the absorption spectra of **PDI-HIPs** indicate the isolated nature of PDIs without any $\pi-\pi$ stacking interactions (Figures S7−S9). This is further supported by 1.5 times higher absorbance of the 0−0 transition than 0−1 (Figure 3a and Figures S7−S9). A further increase in vol % of IPA in water resulted in the decrease of monomer absorbance between 400 and 550 nm, and the appearance of a broad peak above 550 nm indicated the presence of $\pi-\pi$ stacking interactions among PDIs (Figure 3a and Figures S7−S9). The behavior of **PDI-HIPs** is also similar in THF−water mixtures as evidenced by the changes in the electronic absorption spectra (Figure S10). The assembly−disassembly of PDIs in **PDI-HIPs** depending on the solvent composition is further supported by the high fluorescence intensity of PDIs in a 60 vol % amphiphilic solvent (IPA or THF) in water compared to pure water or in an above 90 vol % amphiphilic solvent (THF or IPA) in water (Figure 3b and Figures S8−S10). Moreover, the solution photographs of **PDI-HIPs** taken in water having various vol % of amphiphilic organic solvents (IPA or THF) also support the observations made from absorption and emission spectroscopy (Figure 3c,d and Figures S8−S10). The photographs of assemblies of **PDI-HIPs** in water and in an above 90 vol % amphiphilic solvent (THF or IPA) in water show a visible color change compared to the solutions of isolated PDIs having a 60 vol % amphiphilic solvent (THF or IPA) in water (Figure 3c and Figures S8−S10). As expected, under UV light, **PDI-HIPs** having a 60 vol % amphiphilic solvent (THF or IPA) in water show bright fluorescence owing to the isolated nature of PDIs compared to their assembled state in pure water and water having a more than 90 vol % amphiphilic solvent (THF or IPA) (Figure 3d and Figures S8−S10). All the above observations unambiguously prove the modulation of assembly of PDIs in **PDI-HIPs** by modulating the composition of water and amphiphilic organic solvents. The assembly and disassembly of ionic PDIs can be easily expected in the small molecule state. However, in **PDI-HIPs**, PDIs are covalently crosslinked into a porous network. Despite this covalent crosslinking, the change of assembly and disassembly of PDIs depending on the solvent composition is surprising. This clearly indicates the dynamic nature of the **PDI-HIPs** networks, which can reorganize according to the solvent environment.

To further support our observations on **PDI-HIPs**, we have used **B-PDI** as a model compound. From the absorption and emission spectra, we found that **B-PDI** undergoes self-assembly in water and in an above 90 vol % amphiphilic solvent (THF or IPA) in water (Figures S11 and S12). In the solvent mixture having a 60 vol % amphiphilic solvent (THF or IPA) in water, **B-PDI** disassembles into monomers as evidenced by the absorption and emission spectra and photographs of the solutions (Figures S11 and S12). This clearly indicates that the solvent composition-dependent absorption and emission changes observed for **PDI-HIPs** are due to assembly−disassembly of crosslinked PDI in **PDI-HIPs** and not due to any solvatochromic effects.

In order to understand the assembly and disassembly behavior of **PDI-HIPs** in a mixture of solvents, we performed all-atom molecular dynamics (MD) simulations to determine the solvation mechanism and the stability of **PDI-HIPs** at various concentrations of amphiphilic organic solvents in water.[58] For this purpose, we have taken **B-PDI** as shown in Figure S13 and solvated it in 0, 50, and 95 vol % of IPA in water. Figure 4 shows the radial distribution functions (RDF)

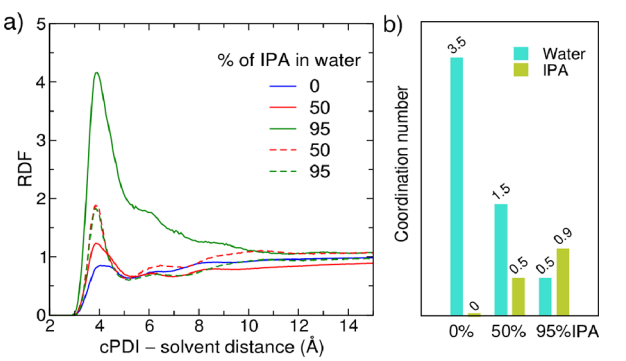

Figure 4. (a) Radial distribution functions (RDF) and (b) coordination numbers between **PDI** ammonium groups and the oxygen of either water (thick line) or IPA (dashed line) molecules at different vol % of IPA in water.

and coordination numbers between PDIs and the solvent obtained from MD simulations (Figure S14). The coordination number is calculated by integrating the RDF up to the first peak maximum (Figure 4b). For the RDF between PDI ammonium groups and water oxygen, with an increase of the vol % of IPA, the intensity of the first peak increases in magnitude while its position changes marginally, and in addition, the peak also becomes broader (Figure 4a). It indicates that water exhibits greater affinity for the ammonium group at 95 vol % of IPA possibly because there are almost no neighboring water molecules that force it to participate in hydrogen bonding with the remaining water molecules. Furthermore, water molecules in the first solvation shell also interact with the carbonyl group through hydrogen bonding (Figure S15). It can be seen from Figure 4b that the corresponding coordination number decreases with increasing

https://doi.org/10.1021/acsapm.2c02102
ACS Appl. Polym. Mater. 2023, 5, 2097−2104

vol % of IPA, indicating the overall decrease of solvation of the ammonium groups. In contrast, the RDF between IPA and ammonium groups shows no change in the intensity of the first maxima while the corresponding coordination number doubles upon increasing the vol % of IPA from 50 to 95 (Figure 4a). The presence of the phenyl ring in the side chain has a minimal impact on the solvation structure surrounding the ammonium group.[50] Further, we calculated the spatial distribution function (SDF) that shows the average density distribution of solvent molecules in a three-dimensional space around the solute. Figure 5 displays the SDF of water (green) and IPA (pink)

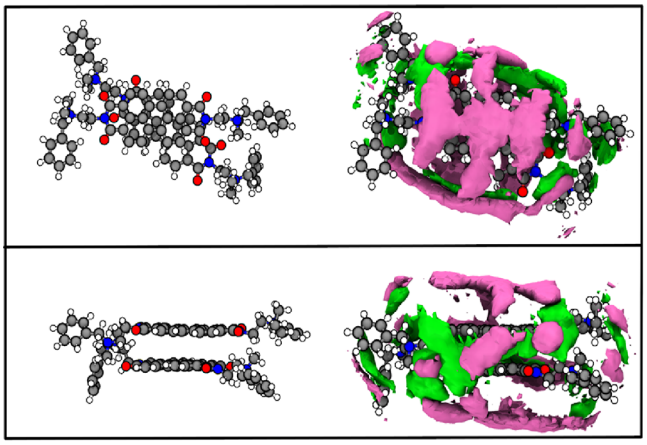

Figure 5. Spatial distribution of solvent molecules (color code for the density: green - water and pink - IPA) around the PDI dimer in 95% IPA in water as obtained from the molecular dynamics simulations. Top and bottom panels show the PDI dimer in top and side views, without and with a density map. Water and IPA density maps are plotted using the isosurface values of 1.71 and 0.004, respectively. Color code: gray - C; white - H; red - O; blue - N.

around the PDI dimer in 95% IPA in water. It should be noted that a density map cannot be obtained around peripheral side chains due to their flexibility. Figure 5 indicates that the aromatic regions of PDI are solvated by IPA molecules, whereas the periphery of the PDI core is solvated by water molecules.

As evidenced from MD simulations, in pure water, the solvation is mainly around the ionic sites and promotes $\pi-\pi$ stacking among PDIs. On the other hand, in the 1:1 mixture of IPA−water, the IPA molecules are mainly around the hydrophobic PDI cores and benzyl groups, whereas water is again concentrated around ammonium ions (Figures 1 and 5). Due to the solvation of both hydrophobic aromatic cores and hydrophilic ionic groups, PDIs exist as monomers without any $\pi-\pi$ stacking interactions consistent with experimental observations. In 95% IPA in water, the solvation of ionic groups and the π surface of PDI are limited, and as a result, restacking of PDIs takes place. Here, it is important to note that, unless the **PDI-HIP** networks are dynamic, the assembly and disassembly of PDIs in **PDI-HIPs** are not feasible. Hence, our experimental and theoretical studies uncover the dynamic nature of HIPs. These are further supported by different degrees of swelling of **PDI-HIPs** depending on the nature of the solvent and the state of PDI in **PDI-HIPs** (Figure 6). To study the swelling behavior, solvents such as water or IPA or the water−IPA mixture were added to **PDI-HIPs** and sonicated to have a proper mixing of the solvent and polymers. The solvent was added to a fixed amount of **PDI-HIPs** until

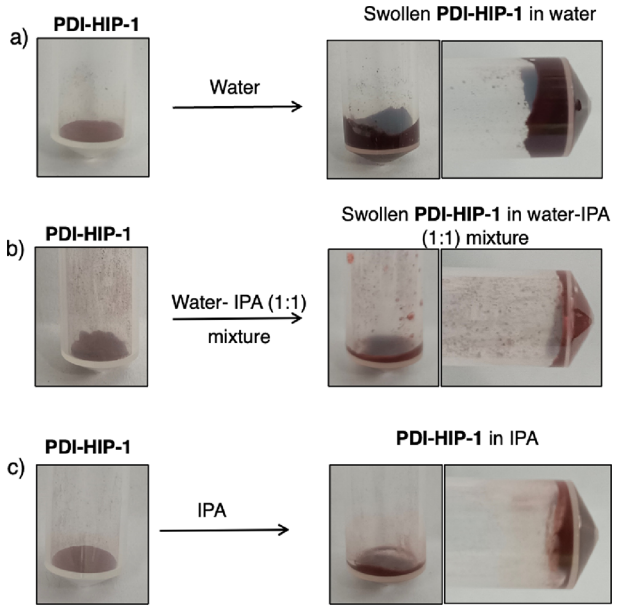

Figure 6. Photographs showing the swelling behavior of **PDI-HIP-1** (a) in water, (b) in a 1:1 water−IPA mixture, and (c) in IPA.

there was no leaking of the solvent when the sample vial was tilted (Figure 6). Interestingly, all the **PDI-HIPs** exhibited strong uptake of water up to 7 (70 mg of water for 10 mg of **PDI-HIP**) times their weight (Table 2). However, the solvent

Table 2. Summary of Solvent Uptake Capacities of PDI-HIPs

	water/**PDI-HIPs** (wt/wt)	water−IPA 1:1 mixture/**PDI-HIPs** (wt/wt)	IPA/PDI-HIPs (wt/wt)
PDI-HIP-1	7	4.5	3.5
PDI-HIP-2	7	3.6	3.1
PDI-HIP-3	6	3.6	3.1

uptake is decreased significantly for a 1:1 water−IPA mixture followed by pure IPA compared to water alone (Table 2). This is due to the higher coordination number for water molecules in **PDI-HIPs** compared to IPA as evidenced from MD simulations (Figure 4b). This is further supported by a significant volume increase of **PDI-HIPs** in water due to swelling compared to the 1:1 water−IPA mixture and IPA (Figure 6). The macroscopic swelling behavior of **PDI-HIPs** also further confirms their dynamic nature. Although swelling behavior was previously observed for few HPCs in organic solvents, molecular-level insights as discussed in this manuscript are missing.[31]

The porous nature and presence of polar functional groups in **PDI-HIPs** further encouraged us to investigate their CO_2 adsorption capacity at 273 K. **PDI-HIP-1**, which possesses the highest surface area, exhibits the highest CO_2 uptake of 2.11 mmol/g (Figure 7). Of the three HCPs studied here, **PDI-HIP-1** has the highest fraction of ultramicropores (<0.7 nm) (Figure 2c). In terms of pore sizes, ultramicropores are the most favorable adsorption sites for CO_2, and the presence of these ultramicropores in **PDI-HIP-1** results in steep CO_2 uptake at low relative pressures. Plots of the specific surface area and the micropore surface area against the amount of CO_2

https://doi.org/10.1021/acsapm.2c02102
ACS Appl. Polym. Mater. 2023, 5, 2097−2104

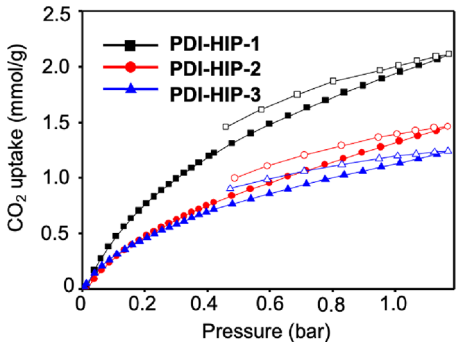

Figure 7. Volumetric CO_2 adsorption (closed symbols) and desorption (open symbols) isotherms of **PDI-HIPs** at 273 K.

adsorbed at a given pressure (~1.17 bar) reveal an almost linear relationship for CO_2 uptake with a specific surface area (Figures S16 and S17). It should be noted that although the surface areas of our **PDI-HIPs** are relatively lower, their CO_2 uptake capacities are comparable to PIPs,[59] COFs,[60] and HIPs[61,62] (Table S3 and Figure S18). This can be attributed to the presence of ultramicropores, which helps to adsorb CO_2 even at low relative pressures (Figure 3c and Figure S17). Moreover, the presence of CO_2-philic polar functional groups such as ammonium and imide also increase the uptake of CO_2 gas in **PDI-HIPs** (Figure S18).

CONCLUSIONS

We have designed and synthesized dynamic HIPs having visible-light absorbing PDIs in a one-pot synthesis through the copolymerization of PDI and DBX. Additionally, we have also provided an approach for understanding the dynamic nature of hyper-crosslinked polymers using ionic PDI as a probe. The polymers exhibit good dispersibility in polar solvents such as water and DMSO. Interestingly, owing to the dynamic nature of the **PDI-HIP** network, PDIs assemble through $\pi-\pi$ stacking in both water and amphiphilic organic solvents and exist as isolated PDIs in their mixtures. This is due to the fact that the ionic part is effectively solvated by water molecules and the hydrophobic part by hydrocarbon chains of amphiphilic organic solvents, as demonstrated by molecular dynamics simulations. As a result of the strong coordination between water and **PDI-HIPs**, their water uptake could reach seven times their weight. Additionally, these polymers exhibit excellent CO_2 uptake up to 2.11 mmol/g at 273 K and 1.17 bar despite their relatively low surface areas compared to various other porous materials (Figure S18). The approach presented in this manuscript is useful for synthesizing various HIPs having large π systems with potential applications in the field of photocatalysis and optoelectronics. We believe that aside from the ease of synthesis of HIPs with tunable surface areas, the properties (dynamic, strong visible-light absorption and solvent composition-modulated assembly) reported here will expand their scope and applications in various fields of materials science.[63,64]

ASSOCIATED CONTENT

Supporting Information

The Supporting Information is available free of charge at https://pubs.acs.org/doi/10.1021/acsapm.2c02102.

Full experimental details, synthesis of **PDI-HIPs** and **B-PDI**, characterization data, TGA data, FT-IR data, and computational details, including Figures S1−S18 and Tables S1−S3 (PDF)

AUTHOR INFORMATION

Corresponding Author

Venkata Rao Kotagiri − *Department of Chemistry, Indian Institute of Technology Hyderabad, Sangareddy, Telangana 502285, India;* orcid.org/0000-0002-6188-4212; Email: kvrao@chy.iith.ac.in

Authors

Soujanya H. Goudar − *Department of Chemistry, Indian Institute of Technology Hyderabad, Sangareddy, Telangana 502285, India*

Dhiraj S. Ingle − *Department of Chemistry, Indian Institute of Technology Hyderabad, Sangareddy, Telangana 502285, India*

Rahul Sahu − *Centre for Computational and Data Science, Indian Institute of Technology Kharagpur, Kharagpur, West Bengal 721302, India*

Srinu Kotha − *Department of Chemistry, Indian Institute of Technology Hyderabad, Sangareddy, Telangana 502285, India*

Sandeep K. Reddy − *Centre for Computational and Data Science, Indian Institute of Technology Kharagpur, Kharagpur, West Bengal 721302, India;* orcid.org/0000-0002-1458-6853

Deepu J. Babu − *Department of Materials Science and Metallurgical Engineering, Indian Institute of Technology Hyderabad, Sangareddy, Telangana 502285, India;* orcid.org/0000-0003-2593-4013

Complete contact information is available at: https://pubs.acs.org/10.1021/acsapm.2c02102

Author Contributions

The manuscript was written through contributions of all authors. All authors have given approval to the final version of this manuscript.

Notes

The authors declare no competing financial interest.

ACKNOWLEDGMENTS

K.V.R. acknowledges the SERB-Early Career Research Award (grant no. ECR/2018/001222), Government of India for financial support. S.H.G. and S.K. thank the CSIR, India for the senior research fellowship. D.S.I. and A.Y. acknowledge funding from the Ministry of Education (MoE) for pursuing PhD. S.K.R. acknowledges the National Supercomputing Mission (NSM) for providing computing resources of "PARAM Shakti" at IIT Kharagpur, which is implemented by C-DAC and supported by the Ministry of Electronics and Information Technology (MeitY) and the Department of Science and Technology (DST), Government of India. S.K.R. acknowledges the ISIRD award, IIT Kharagpur for financial support. R.S. thanks the UGC, India for the senior research fellowship. D.J.B. acknowledges SERB (grant no. SRG/2021/000731), Government of India for financial support. We thank Mr. Aditya Yadav for the SEM measurements.

REFERENCES

(1) Slater, A. G.; Cooper, A. I. Function-Led Design of New Porous Materials. *Science* **2015**, *348*, 8075.

(2) Mohamed, M. G.; El-Mahdy, A. F. M.; Kotp, M. G.; Kuo, S. W. Advances in Porous Organic Polymers: Syntheses, Structures, and Diverse Applications. *Mater. Adv.* **2022**, *3*, 707−733.
(3) Makal, T. A.; Li, J. R.; Lu, W.; Zhou, H. C. Methane Storage in Advanced Porous Materials. *Chem. Soc. Rev.* **2012**, *41*, 7761−7779.
(4) Chang, Z.; Zhang, D. S.; Chen, Q.; Bu, X. H. Microporous Organic Polymers for Gas Storage and Separation Applications. *Phys. Chem. Chem. Phys.* **2013**, *15*, 5430−5442.
(5) Jia, D.; Ma, L.; Wang, Y.; Zhang, W.; Li, J.; Zhou, Y.; Wang, J. Efficient CO_2 Enrichment and Fixation by Engineering Micropores of Multifunctional Hypercrosslinked Ionic Polymers. *Chem. Eng. J.* **2020**, *390*, No. 124652.
(6) Lu, Y.; Liu, W.; Liu, J.; Li, X.; Zhang, S. A Review on 2D Porous Organic Polymers for Membrane-Based Separations: Processing and Engineering of Transport Channels. *Adv. Membr.* **2021**, *1*, No. 100014.
(7) Zhang, Y.; Riduan, S. N. Functional Porous Organic Polymers for Heterogeneous Catalysis. *Chem. Soc. Rev.* **2012**, *41*, 2083−2094.
(8) Wang, S.; Li, H.; Huang, H.; Cao, X.; Chen, X.; Cao, D. Porous Organic Polymers as a Platform for Sensing Applications. *Chem. Soc. Rev.* **2022**, *51*, 2031−2080.
(9) Liu, X.; Liu, C. F.; Xu, S.; Cheng, T.; Wang, S.; Lai, W. Y.; Huang, W. Porous Organic Polymers for High-Performance Supercapacitors. *Chem. Soc. Rev.* **2022**, *51*, 3181−3225.
(10) Feng, X.; Ding, X.; Jiang, D. Covalent Organic Frameworks. *Chem. Soc. Rev.* **2012**, *41*, 6010−6022.
(11) Sci, C.; Jiang, J.; Trewin, A.; Adams, D. J.; Cooper, A. I. Band Gap Engineering in Fluorescent Conjugated Microporous Polymers. *Chem. Sci.* **2011**, *2*, 1777−1781.
(12) Lee, J. S. M.; Cooper, A. I. Advances in Conjugated Microporous Polymers. *Chem. Rev.* **2020**, *120*, 2171−2214.
(13) Song, Y.; Lan, P. C.; Martin, K.; Ma, S. Rational Design of Bifunctional Conjugated Microporous Polymers. *Nanoscale Adv.* **2021**, *3*, 4891−4906.
(14) Ben, T.; Qiu, S. Porous Aromatic Frameworks: Synthesis Structure and Functions. *CrystEngComm* **2013**, *15*, 17−26.
(15) Budd, P. M.; Ghanem, B. S.; Makhseed, S.; McKeown, N. B.; Msayib, K. J.; Tattershall, C. E. Polymers of Intrinsic Microporosity (PIMs): Robust, Solution-Processable Organic Nanoporous Materials. *Chem. Commun.* **2004**, *4*, 230−231.
(16) Msayib, K. J.; McKeown, N. B. Inexpensive Polyphenylene Network Polymers with Enhanced Microporosity. *J. Mater. Chem. A* **2016**, *4*, 10110−10113.
(17) Wood, C. D.; Bien, T.; Trewin, A.; Hongjun, N.; Bradshaw, D.; Rosseinsky, M. J.; Khimyak, Y. Z.; Campbell, N. L.; Kirk, R.; Stöckel, E.; Cooper, A. I. Hydrogen Storage in Microporous Hypercrosslinked Organic Polymer Networks. *Chem. Mater.* **2007**, *19*, 2034−2048.
(18) Alahmed, A. H.; Briggs, M. E.; Cooper, A. I.; Adams, D. J. Covalent and Electrostatic Incorporation of Amines into Hypercrosslinked Polymers for Increased CO_2 Selectivity. *J. Polym. Sci. Part A. Polym. Chem.* **2018**, *56*, 2513−2521.
(19) Li, J.; Han, Y.; Lin, H.; Wu, N.; Li, Q.; Jiang, J.; Zhu, J. Cobalt-Salen-Based Porous Ionic Polymer: The Role of Valence on Cooperative Conversion of CO_2 to Cyclic Carbonate. *ACS Appl. Mater. Interfaces* **2020**, *12*, 609−618.
(20) Tsyurupa, M. P.; Davankov, V. A. Hypercrosslinked Polymers: Basic Principle of Preparing the New Class of Polymeric Materials. *React. Funct. Polym.* **2002**, *53*, 193−203.
(21) Wang, L.; Wan, Y.; Ding, Y.; Wu, S.; Zhang, Y.; Zhang, X.; Zhang, G.; Xiong, Y.; Wu, X.; Yang, J.; Xu, H. Conjugated Microporous Polymer Nanosheets for Overall Water Splitting Using Visible Light. *Adv. Mater.* **2017**, *29*, No. 1702428.
(22) Ren, S.; Dawson, R.; Adams, D. J.; Cooper, A. I. Low Band-Gap Benzothiadiazole Conjugated Microporous Polymers. *Polym. Chem.* **2013**, *4*, 5585−5590.
(23) Li, L.; Cai, Z.; Wu, Q.; Lo, W. Y.; Zhang, N.; Chen, L. X.; Yu, L. Rational Design of Porous Conjugated Polymers and Roles of Residual Palladium for Photocatalytic Hydrogen Production. *J. Am. Chem. Soc.* **2016**, *138*, 7681−7686.
(24) Rao, K. V.; Haldar, R.; Maji, T. K.; George, S. J. Dynamic, Conjugated Microporous Polymers: Visible Light Harvesting via Guest-Responsive Reversible Swelling. *Phys. Chem. Chem. Phys.* **2016**, *18*, 156−163.
(25) Rao, K. V.; Mohapatra, S.; Maji, T. K.; George, S. J. Guest-Responsive Reversible Swelling and Enhanced Fluorescence in a Super-Absorbent, Dynamic Microporous Polymer. *Chem. - Eur. J.* **2012**, *18*, 4505−4509.
(26) Xiao, R.; Tobin, J. M.; Zha, M.; Hou, Y. L.; He, J.; Vilela, F.; Xu, Z. A Nanoporous Graphene Analog for Superfast Heavy Metal Removal and Continuous-Flow Visible-Light Photoredox Catalysis. *J. Mater. Chem. A* **2017**, *5*, 20180−20187.
(27) Taylor, D.; Hu, X.; Wu, C. M.; Tobin, J. M.; Oriou, Z.; He, J.; Xu, Z.; Vilela, F. Superprotonic Conduction of Intrinsically Zwitterionic Microporous Polymers Based on Easy-to-Make Squaraine Croconaine and Rhodizaine Dyes. *Nanoscale Adv.* **2022**, *4*, 2922−2928.
(28) Cui, D.; Yao, C.; Xu, Y. Conjugated Microporous Polymers with Azide Groups: A New Strategy for Postsynthetic Fluoride Functionalization and Effectively Enhanced CO_2 Adsorption Properties. *Chem. Commun.* **2017**, *53*, 11422−11425.
(29) Wang, S.; Zhang, C.; Shu, Y.; Jiang, S.; Xia, Q.; Chen, L.; Jin, S.; Hussain, I.; Cooper, A. I.; Tan, B. Layered Microporous Polymers by Solvent Knitting Method. *Sci. Adv.* **2017**, *3*, No. 1602610.
(30) Li, B.; Guan, Z.; Yang, X.; Wang, W. D.; Hussain, I.; Song, K.; Tan, B.; Li, T. Multifunctional Microporous Organic Polymers. *J. Mater. Chem. A* **2014**, *2*, 11930−11939.
(31) Wilson, C.; Main, M. J.; Cooper, N. J.; Briggs, M. E.; Cooper, A. I.; Adams, D. J. Swellable Functional Hypercrosslinked Polymer Networks for the Uptake of Chemical Warfare Agents. *Polym. Chem.* **2017**, *8*, 1914−1922.
(32) Li, J.; Jia, D.; Guo, Z.; Liu, Y.; Lyu, Y.; Zhou, Y.; Wang, J. Imidazolinium Based Porous Hypercrosslinked Ionic Polymers for Efficient CO_2 Capture and Fixation with Epoxides. *Green Chem.* **2017**, *19*, 2675−2686.
(33) Schukraft, G. E. M.; Woodward, R. T.; Kumar, S.; Sachs, M.; Eslava, S.; Petit, C. Hypercrosslinked Polymers as a Photocatalytic Platform for Visible-Light-Driven CO_2 Photoreduction Using H_2O. *ChemSusChem* **2021**, *14*, 1720−1727.
(34) Li, X.; Chen, G.; Xu, H.; Jia, Q. Task-Specific Synthesis of Cost-Effective Electron-Rich Thiophene-Based Hypercrosslinked Polymer with Perylene for Efficient Iodine Capture. *Sep. Purif. Technol.* **2019**, *228*, No. 115739.
(35) Nielsen, C. B.; Holliday, S.; Chen, H. Y.; Cryer, S. J.; McCulloch, I. Non-Fullerene Electron Acceptors for Use in Organic Solar Cells. *Acc. Chem. Res.* **2015**, *48*, 2803−2812.
(36) Hou, J.; Inganas, O.; Friend, R. H.; Gao, F. Organic Solar Cells Based on Non-Fullerene Acceptors. *Nat. Mater.* **2018**, *17*, 119−128.
(37) Kaur, S.; Kumar, M.; Bhalla, V. Supramolecular ensemble of PBI derivative and copper nanoparticles: A light harvesting antenna for photocatalyticC(sp2)-H functionalization. *Green Chem.* **2016**, *18*, 5870−5883.
(38) Manoj, T.; Kotha, S.; Paikaray, B.; Srideep, D.; Haldar, A.; Rao, K. V.; Murapaka, C. Giant Spin Pumping at the Ferromagnet (Permalloy)-Organic Semiconductor (Perylene Diimide) Interface. *RSC Adv.* **2021**, *11*, 35567−35574.
(39) Zhang, F.; Ma, Y.; Chi, Y.; Yu, H.; Li, Y.; Jiang, T.; Wei, X.; Shi, J. Self-Assembly, Optical and Electrical Properties of Perylene Diimide Dyes Bearing Unsymmetrical Substituents at Bay Position. *Sci. Rep.* **2018**, *8*, 8208.
(40) Würthner, F.; Bauer, C.; Stepanenko, V.; Yagai, S. A Black Perylene Bisimide Super Gelator with an Unexpected J-Type Absorption Band. *Adv. Mater.* **2008**, *20*, 1695−1698.
(41) Perez, G. S.; Dasgupta, S.; Żuraw, W.; Pineda, R. F.; Wojciechowski, K.; Jagadamma, L. K.; Samuel, I.; Robertson, N. Solution-Processable Perylene Diimide-Based Electron Transport Materials as Non-Fullerene Alternatives for Inverted Perovskite Solar Cells. *J. Mater. Chem. A* **2022**, 11046−11053.

https://doi.org/10.1021/acsapm.2c02102
ACS Appl. Polym. Mater. 2023, 5, 2097−2104

(42) Cao, J.; Yang, S. Progress in Perylene Diimides for Organic Solar Cell Applications. *RSC Adv.* **2022**, *12*, 6966−6973.
(43) Rajaram, S.; Shivanna, R.; Kandappa, S. K.; Narayan, K. S. Nonplanar Perylene Diimides as Potential Alternatives to Fullerenes in Organic Solar Cells. *J. Phys. Chem. Lett.* **2012**, *3*, 2405−2408.
(44) Rao, K. V.; Haldar, R.; Kulkarni, C.; Maji, T. K.; George, S. J. Perylene Based Porous Polyimides: Tunable, High Surface Area with Tetrahedral and Pyramidal Monomers. *Chem. Mater.* **2012**, *24*, 969−971.
(45) Rao, K. V.; Haldar, R.; Maji, T. K.; George, S. J. Porous Polyimides from Polycyclic Aromatic Linkers: Selective CO_2 Capture and Hydrogen Storage. *Polymer* **2014**, *55*, 1452−1458.
(46) Liebl, M. R.; Senker, J. Microporous Functionalized Triazine-Based Polyimides with High CO_2 Capture Capacity. *Chem. Mater.* **2013**, *25*, 970−980.
(47) Narzary, B. B.; Baker, B. C.; Yadav, N.; D'Elia, V.; Faul, C. F. J. Crosslinked Porous Polyimides: Structure Properties and Applications. *Polym. Chem.* **2021**, *12*, 6494−6514.
(48) Li, L.; Cai, Z. Structure control and photocatalytic performance of porous conjugated polymers based on perylene diimide. *Polym. Chem.* **2016**, *7*, 4937−4943.
(49) Jin, S.; Supur, M.; Addicoat, M.; Furukawa, K.; Chen, L.; Nakamura, T.; Fukuzumi, S.; Irle, S.; Jiang, D. Creation of Superheterojunction Polymers Via Direct Polycondensation: Segregated and Bicontinuous Donor-Acceptor π-Columnar Arrays in Covalent Organic Frameworks for Long-Lived Charge Separation. *J. Am. Chem. Soc.* **2015**, *137*, 7817−7827.
(50) Kotha, S.; Mabesoone, M. F. J.; Srideep, D.; Sahu, R.; Reddy, S. K.; Rao, K. V. Supramolecular Depolymerization in the Mixture of Two Poor Solvents: Mechanistic Insights and Modulation of Supramolecular Polymerization of Ionic π-Systems. *Angew. Chemi.* **2021**, *60*, 5459−5466.
(51) Lafleur, R. P. M.; Lou, X.; Pavan, G. M.; Palmans, A. R. A.; Meijer, E. W. Consequences of a Cosolvent on the Structure and Molecular Dynamics of Supramolecular Polymers in Water. *Chem. Sci.* **2018**, *9*, 6199−6209.
(52) Martínez, M. A.; Doncel-Giménez, A.; Cerdá, J.; Calbo, J.; Rodríguez, R.; Aragó, J.; Crassous, J.; Ortí, E.; Sánchez, L. Distance Matters: Biasing Mechanism, Transfer of Asymmetry, and Stereomutation in N-Annulated Perylene Bisimide Supramolecular Polymers. *J. Am. Chem. Soc.* **2021**, *143*, 13281−13291.
(53) Bejagam, K. K.; Fiorin, G.; Klein, M. L.; Balasubramanian, S. Supramolecular Polymerization of Benzene-1,3,5-Tricarboxamide: A Molecular Dynamics Simulation Study. *J. Phys. Chem. B.* **2014**, *118*, 5218−5228.
(54) Korlepara, D. B.; Bejagam, K. K.; Balasubramanian, S. Supramolecular Polymerization of N,N,N,N-Tetra-(Tetradecyl)-1,3,6,8-Pyrenetetracarboxamide: A Computational Study. *J. Phys. Chem. B.* **2017**, *121*, 11492−11503.
(55) De Marco, A. L.; Bochicchio, D.; Gardin, A.; Doni, G.; Pavan, G. M. Controlling Exchange Pathways in Dynamic Supramolecular Polymers by Controlling Defects. *ACS Nano* **2021**, *15*, 14229−14241.
(56) Thommes, M.; Kaneko, K.; Neimark, A. V.; Olivier, J. P.; Rodriguez-Reinoso, F.; Rouquerol, J.; Sing, K. S. W. Physisorption of Gases, with Special Reference to the Evaluation of Surface Area and Pore Size Distribution. *Pure Appl. Chem.* **2015**, *87*, 1051−1069.
(57) Yu, S. B.; Lin, F.; Tian, J.; Yu, J.; Zhang, D. W.; Li, Z. T. Water-Soluble and Dispersible Porous Organic Polymers: Preparation Functions and Applications. *Chem. Soc. Rev.* **2022**, *51*, 434−449.
(58) Abraham, M. J.; Murtola, T.; Schulz, R.; Páll, S.; Smith, J. C.; Hess, B.; Lindah, E. Gromacs: High Performance Molecular Simulations through Multi-Level Parallelism from Laptops to Supercomputers. *SoftwareX.* **2015**, *1−2*, 19−25.
(59) Sun, Q.; Jin, Y.; Aguila, B.; Meng, X.; Ma, S.; Xiao, F. S. Porous Ionic Polymers as a Robust and Efficient Platform for Capture and Chemical Fixation of Atmospheric CO_2. *ChemSusChem* **2017**, *10*, 1160−1165.
(60) Chandra, S.; Kandambeth, S.; Biswal, B. P.; Lukose, B.; Kunjir, S. M.; Chaudhary, M.; Babarao, R.; Heine, T.; Banerjee, R. Chemically Stable Multilayered Covalent Organic Nanosheets from Covalent Organic Frameworks via Mechanical Delamination. *J. Am. Chem. Soc.* **2013**, *135*, 17853−17861.
(61) Sang, Y.; Shu, Z.; Wang, Y.; Wang, L.; Zhang, D.; Xiao, Q.; Zhou, F.; Huang, J. Bifunctional Ionic Hyper-Cross-Linked Polymers for CO2 Capture and Catalytic Conversion. *Appl. Surf. Sci.* **2022**, *585*, No. 152663.
(62) Liu, C.; Shi, L.; Zhang, J.; Sun, J. One-Pot Synthesis of Pyridine-Based Ionic Hyper-Cross-Linked Polymers with Hierarchical Pores for Efficient CO_2 Capture and Catalytic Conversion. *Chem. Eng. J.* **2022**, *427*, No. 131633.
(63) Xu, D.; Guo, J.; Yan, F. Porous Ionic Polymers: Design, Synthesis, and Applications. *Prog. Polym. Sci.* **2018**, *79*, 121−143.
(64) Mal, A.; Vijayakumar, S.; Mishra, R. K.; Jacob, J.; Pillai, R. S.; Dileep Kumar, B. S.; Ajayaghosh, A. Supramolecular Surface Charge Regulation in Ionic Covalent Organic Nanosheets: Reversible Exfoliation and Controlled Bacterial Growth. *Angew. Chem.* **2020**, *59*, 8713−8719.